

The eigenmode frequency distribution of rapidly rotating neutron stars

Stratos Boutloukos and Hans-Peter Nollert

*Theoretical Astrophysics, University of Tübingen, Auf der Morgenstelle 10, 72076, Tübingen, D**

(Dated: December 2, 2024)

We use perturbation theory and the relativistic Cowling approximation to numerically compute characteristic oscillation modes of rapidly rotating relativistic stars which consist of a perfect fluid obeying a polytropic equation of state. We find the expected infinite pressure mode spectrum extending towards higher frequencies, but also what appears to be an infinite number of inertial modes confined to a finite, well-defined frequency range, depending on the compactness and the rotation frequency of the star. We observe the shift of this range towards negative frequencies for non-axisymmetric modes with respect to the axisymmetric ones, making all $m > 2$ modes unstable. We discuss whether our results indicate the existence of a continuous part of the star's spectrum, or whether they all are discrete solutions.

I. INTRODUCTION

Helioseismology and asteroseismology have provided a wealth of information about our sun, early type variable stars and even white dwarfs [see 28, chap. 2]. However, for neutron stars, this field is still at its beginning, since it is very difficult to measure their oscillation modes in the electromagnetic spectrum. The gravitational wave spectrum, though, will likely allow us to study neutron star oscillations and obtain information about their parameters, such as mass, radius, rotation rate and equation of state [3]. In this context, a discovery by Andersson [1] caused some excitement: the so-called r -modes may be unstable at any non-zero rotation rate of a compact star. Once excited — e.g. during the birth of a neutron star, via an accretion process, or through tidal interactions with a bound compact object — it may grow to sufficient strength to be detected by an earth-bound gravitational wave detector [2]. This mechanism, the so-called CFS instability [13], may cause the fundamental pressure mode (f -mode) of a neutron star to become unstable as well. However, this occurs only when the rotation frequency of the star is close to the Kepler limit [30]. Many gravity modes (g -modes) can become unstable as well, although their growth is most likely suppressed by viscous dissipation [16]. The latter are related to either composition gradient or finite temperature, which are not considered in this work.

We concentrate here on isentropic models, where a star's equilibrium as well as its perturbations can be described with the same one-parameter equation of state $p = p(e)$ and constant entropy [20] (also called barotropic [19]). Deviations from an isentropic model become important only if the epicyclic spin frequency is comparable to or smaller than the Brunt-Väisälä frequency, which for neutron stars is on the order of 100Hz [18].

Originally defined based on Newtonian models, r -modes and g -modes differ in parity: inertial modes with axial parity under space inversions are considered r -

modes, those with polar parity g -modes [32]. For relativistic models this definition does not hold any more since oscillation modes (except dipole modes) do not have unique parity. Instead, a mixture of the two parities is observed, leading to 'hybrid' modes [20]. Instead one speaks about 'generalized r -modes' where the leading order term, if the velocity field is decomposed into a sum of spherical harmonic functions, has axial parity, and about generalized g -modes if the leading order term has polar-parity. Generalized r -modes have frequencies to about 20-30% lower than their Newtonian counterparts[18].

In non-rotating isentropic stars, the (generalized) r -modes as well as the g -modes are degenerate due to the absence of their restoring forces, the Coriolis force and buoyancy respectively. Rotation breaks this degeneracy and this large subspace of modes, which have finite frequencies now, form the set of inertial modes. There is an infinite number of inertial modes for relativistic isentropic stars [19]. To our knowledge the range of frequencies they cover has been studied only for Newtonian incompressible stars [17]: The analytic solutions extend from $(-2 - m)\nu$ to $(2 - m)\nu$ where ν is the rotational frequency of the star and m the azimuthal index. Later Brink et al. [7] computed a large set of such modes in the same framework and confirmed modes up to 30th order to have frequencies confined within this range. Ruoff et al. [25] studied the inertial mode spectrum for relativist barotropic (as well as non-barotropic) stars in the slow-rotation approximation by including coupling of modes up to a maximum harmonic index ℓ_{max} . Next to distinct inertial modes they found a continuous spectrum whose width depends on the compactness of the star and on ℓ_{max} . They all lie roughly between $-\nu$ and ν for $m = 0$ and between -2ν and 0 for $m = 2$. For $\ell_{max} \rightarrow \infty$ the authors expect the continuous spectrum to fully cover this range with individual modes still existing inside the continuous spectrum. On the other hand, Lockitch et al. [19] argue in their appendix that only individual modes should be present.

All stars show pressure driven modes (p -modes). The fundamental p -mode, having the lowest frequency, is called the f -mode. They were studied first in non-rotating models. In Newtonian gravity the perturba-

*Electronic address: stratos@tat.physik.uni-tuebingen.de

tion equation describing their frequencies is of Sturm-Liouville type [see eg. 8], the solution is an infinite set of modes with frequency range unbound from above. General relativity and rotation do not change this general picture, and individual frequencies are only slightly affected for a spin frequency up to about half the break-up frequency [10]. The f -mode typically has a frequency around 2kHz, the lowest order p -mode a somewhat higher one. For a review regarding fluid oscillations of neutron stars see [23] and [14], [27] for rotating neutron stars, and [4] for r -modes.

Most studies of neutron star oscillations use the so-called Cowling approximation where one looks only at fluid displacements and neglects metric perturbations [8]. Lockitch et al. [18] consider the results of Ruoff et al. [25] unreliable due to its use. Yoshida et al. [31], however, found what they identify as the fundamental r -mode to deviate only a few percent of the rotational frequency of the star from the modes calculated without the Cowling approximation in the slow-rotation regime. This confirmed earlier results from Provost et al. [24]. Thus, although Finn [12] showed that one should not use the relativistic Cowling approximation for calculating g -modes (which have low frequency and involve large fluid velocities), it appears that for r -modes, which have similar properties, frequencies can be calculated fairly accurately with this approach. Furthermore, the Cowling approximation has been shown [29] to give accurate results (up to about 20%) for relativistic non-radial p -modes.

On the other hand, using the slow-rotation approximation may be more problematic than the Cowling approximation. It seems that going beyond the first order in the rotation rate of the star, results may differ considerably from those obtained in first order [5]. Therefore, in this paper we will discard the slow-rotation limit, performing mode calculations for rapidly rotating stars using linear perturbation theory in the Cowling approximation in relativistic rather than Newtonian gravity. Given the results discussed above, we expect to come against an infinite number of pressure modes with frequencies on the order of kHz and higher, and possibly an infinite number of hybrid (mixed parity) inertial modes, with frequencies dependent on the rotation rate of the star.

In section II we formulate the problem and discuss the numerical setup. In section III we investigate axisymmetric perturbations, first in the non-rotating case for comparison with known results, and then for the rotating case. Results for non-axisymmetric perturbations and a comparison with the axisymmetric ones follow in section IV, concluding with a discussion of the results in Section V.

II. PROBLEM SET-UP

A. Equilibrium background

Neutron stars have been observed to spin up to millisecond periods. This results in significant deviations from spherical symmetry both for the fluid configuration of the star and for the spacetime. Equilibrium solutions will thus not be spherically symmetric, but axisymmetric at most. The general form of an axisymmetric metric describing a rotating body can be written as:

$$ds^2 = -e^{\gamma+\rho} dt^2 + e^{2\alpha} (dr^2 + r^2 d\theta^2) + e^{\gamma-\rho} r^2 \sin^2 \theta (d\phi - \omega dt)^2. \quad (1)$$

where r, θ, ϕ are quasi-isotropic coordinates, reducing to isentropic ones for no rotation [see 27]. Restricting ourselves to uniform rotation with frequency Ω , the 4-velocity of the fluid is given by $u^\alpha = U^0 \{1, 0, 0, \Omega\}$, with an energy-moment tensor $T_{\mu\nu} = p g_{\mu\nu} + (p + \epsilon) U_\mu U_\nu$, assuming that the star consists of an ideal fluid. For the equation of state we use a simple polytropic model of the form $p = k \times \rho_0^\gamma$. Using a realistic equation of state in tabulated form would not affect our analysis or our numerical procedure. In this paper, we restrict ourselves to a polytropic equation of state to facilitate comparison of our results with previous studies by other authors.

We use the RNS code of Stergioulas & Friedman [26] for computing the background models. The same code was also used by Font et al. [10]; we will occasionally refer to their results for comparison. Table I summarizes some of their models which we will be using here. For all models, the parameters in the equation of state are $k = 217.856 \text{ km}^2$ and $\gamma = 2$; the central density is always $\epsilon_c = 0.894 \times 10^{15} \text{ g/cm}^3$.

TABLE I: The models of Font et al. [10] which we refer to in this paper.

| Model | Gravitational Mass | Radius | Ω | Rot. rate (ν) |
|-------|--------------------|----------|-----------|---------------------|
| BU0 | $1.4M_\odot$ | 14.15 km | 0 | 0 |
| BU1 | $1.432M_\odot$ | 14.51 km | 2.185 kHz | 348Hz |
| BU6 | $1.627M_\odot$ | 17.25 km | 4.984 kHz | 793Hz |

B. Perturbations

Assuming small deviations for the fluid variables we study linearized perturbations on these stationary configurations. Since the background is not spherically symmetric it is not helpful to decompose the perturbations into spherical harmonics. Instead exploit the axisymmetry of the background by writing the perturbation quantities as

$$\delta p = H e^{im\phi} \quad (2a)$$

$$\delta u_\alpha = \frac{1}{p + \epsilon} \{-\Omega f_3, f_1, f_2, f_3\} e^{im\phi}. \quad (2b)$$

The reason for this particular choice will become clear in the next subsection (II C). The perturbation of the energy-density is related to the pressure perturbation through

$$\delta p = \frac{dp}{d\epsilon} \delta \epsilon \equiv C_s^2 \delta \epsilon,$$

where C_s is the speed of sound.

As mentioned earlier we use the Cowling approximation, (Cowling [8] after Emden [11]) neglecting the metric perturbations. This will not allow us to calculate any damping of the modes due to emission of gravitational waves, but we can estimate the oscillation frequencies and study the overall structure of the spectrum (see also section I).

The equations that describe the behavior of the perturbed quantities arise from the perturbed form of the conservation of energy-momentum (equations of motion for the fluid):

$$\delta (T_{\mu;\nu}^\nu) = g^{\kappa\nu} (\delta T_{\mu\kappa,\nu} - \delta T_{\mu\rho} \Gamma_{\nu\kappa}^\rho - \Gamma_{\mu\nu}^\rho \delta T_{\rho\kappa}) = 0 \quad (3)$$

In general, these yield four independent partial differential equations which are of first order in time and space. We perform mode calculations by assuming a harmonic time-dependence $e^{i\sigma t}$ for all four variables (e.g. $\delta p(t, r, \theta, \phi) = \delta p(t, r, \theta) e^{i\sigma t}$), searching for frequencies which allow non-trivial solutions of the perturbation equations.

C. Numerical procedure

Here we briefly describe the numerical method used in this work. We discretize the system of equations at every grid point, including the boundaries by making use of the boundary conditions. This results in a system of linear equations of the form

$$\mathbf{A} \cdot \mathbf{X} = 0 \quad (4)$$

where the unknowns \mathbf{X} are the discrete perturbation quantities at all grid points, and the coefficient matrix \mathbf{A} represents the equations resulting from the perturbation equations at all grid points and from the boundary conditions. \mathbf{A} is a highly sparse matrix. The components of \mathbf{A} depend on the frequency parameter σ . It is now possible to examine the condition of \mathbf{A} , searching for values of σ which make \mathbf{A} degenerate, since this is the only way that Eq. (4) allows non-trivial solutions for the perturbation quantities.

In the case we study here, we may rewrite Eq. (4) as an eigenvalue problem of the form

$$\tilde{\mathbf{A}} \cdot \mathbf{X} = i\sigma \mathbf{X} \quad (5)$$

Note that this is a special case and not generally possible; it will probably not work for the general perturbation equations which result if one does not use the Cowling approximation.

We may now use a standard routine for finding eigenvalues of Eq. (5). We use the routine `cg.f` from the EISPACK package of the NETLIB libraries which handles general complex matrices by use of the QR-algorithm. The characteristic frequencies of the star's oscillation modes are obtained as eigenvalues of Eq. (5), the perturbation quantities \mathbf{X} are the corresponding eigenvalues. It has turned out that a two-sided differencing scheme does not give consistent results (see [6]). We therefore use a one-sided differencing scheme for all first derivatives throughout this work.

We need to take into account boundary conditions at the center and at the surface of the star, and a regularity condition in the angular direction. At the center, all variables are required to vanish by the regularity condition there. We implement this condition simply by setting all variables to zero at $r = 0$. At the surface, all perturbation variables must vanish: this follows from the definition of the variables given in Eqs. (2), since $p = \epsilon = \partial_r p = 0$ (for polytropic equations of state) and $\delta p \sim \partial_r p$ (to first order in a Taylor expansion). For the special case of $m = 0$, the pressure perturbation is not required to vanish at the center; its value must then be determined directly through Eqs. (3).

For the boundaries in the θ -direction one may use the fact that the rotational axis itself is special: For $m > 0$, all variables have to vanish on the rotational axis due to regularity conditions [33]. This can be used directly to set values for the discretized variables there. For $m = 0$ we may construct a grid in such a way that no grid points fall on the rotational axis. In this case, one must use the symmetry condition to construct a boundary condition in the θ -direction. This technique is also applicable for $m > 0$, keeping in mind that the symmetry is different for even and odd values of m . We have used both techniques for the $m = 2$ case and found no significant difference. In order to make the code applicable both in the axisymmetric and the non-axisymmetric case, we implemented the second possibility.

The RNS code itself has finite resolution and thus introduces some numerical error into the results. We will always see a combination of numerical error coming from the RNS code and from our own code. When we attempt to study convergence properties we therefore use a high but fixed resolution of the RNS code, varying only the resolution of our eigenvalue code. In order to avoid the use of interpolation and the additional error associated with it, we run our code only with grid spacings which are multiples of the fixed grid spacing we have chosen for the RNS code.

III. AXISYMMETRIC PERTURBATIONS

We first study axisymmetric perturbations as a test for our code. We use the corresponding equations in their general form, including all terms with arbitrary m . Setting $m = 0$ we select perturbations that are symmetric around the rotation axis, which include all $\ell \geq 0$ contributions. Axisymmetric perturbations have been studied by Font et al. [10] using nonlinear time-evolution; we will turn to their results for comparison. In order to gain a better understanding of the underlying physics and numerics, we first solve Eqs. (3) for the non-rotating case, where expressions can also take a considerably reduced form. We then proceed to include rotation at arbitrary rotation rate.

A. No rotation

Setting $\Omega = 0$ in Eqs. (3) and using harmonic time-dependence the system of equations for the variables defined in Eqs. 2 takes the form:

$$\begin{aligned} i\sigma H &= -\frac{imC_s^2 e^{2\rho} U^0}{r^2 \sin^2 \theta} f_3 - \frac{C_s^2}{e^{2\alpha} U^0} \left\{ \frac{1}{r^2} \left(\frac{\partial f_2}{\partial \theta} + \frac{\cos \theta}{\sin \theta} f_2 \right) \right. \\ &\quad \left. + \frac{\partial f_1}{\partial r} + \left(\frac{3}{2} \frac{\partial \gamma}{\partial r} + \frac{1}{2} \frac{\partial \rho}{\partial r} + \frac{2}{r} \right) f_1 \right\} \\ i\sigma f_3 &= -\frac{im}{U^0} H, \quad i\sigma f_1 = -\frac{1}{U^0} \frac{\partial H}{\partial r}, \quad i\sigma f_2 = -\frac{1}{U^0} \frac{\partial H}{\partial \theta} \quad (6) \end{aligned}$$

In this simple case, one variable (H) would be sufficient to describe the whole oscillation problem since one can transform the system of Eqs. (6) into a single second order equation. Solving the latter gave same results as solving Eqs. (3) for $\Omega = 0$ so we will keep presenting results from the full first-order system for consistency.

Table II shows the lowest resulting eigenfrequencies for the model BU0 with increasing resolution in the radial direction, starting from 21 points. We will be referring from now on the physical oscillation mode frequency, f , rather than the epicyclic one ($\sigma = 2\pi f$) unless stated otherwise. Increasing the resolution in the θ direction does not seem to affect the results, and it is computationally expensive. We therefore keep the θ -resolution fixed for the results shown in Table II.

Figure 1 shows a plot of the ($l = 2, m = 0$) f -mode frequencies from Table II as a function of the radial resolution. They follow an inverse power law of the form $f = f_\infty + \delta f/n_r + \dots$, i.e. first order convergence, as one would expect for one-sided differences. We may thus extrapolate the computed values to obtain an eigenfrequency f_∞ at nominally infinite resolution. In general, the relative mean deviation of the fitted numbers is less than 1%. Note that there is an additional systematic error of the same general magnitude, resulting from the finite accuracy of the background quantities.

Since the background is now spherically symmetric, we can assign a definite value of ℓ to the oscillation modes.

TABLE II: The frequencies ($\frac{\sigma}{2\pi}$) in Hz of the first three fundamental modes (f) and the lowest pressure mode (p^1) for axisymmetric oscillations of BU0, for several resolutions in the radial direction and a fixed number of θ -points. In the next to last row the extrapolated values for 'infinite' r -resolution (see figure 1) are listed, while the last row shows the results of Font et al. [10].

| n_θ | n_r | $f_{\ell=1}$ | $f_{\ell=2}$ | $f_{\ell=0}$ | $p_{\ell=2}^1$ |
|------------------|----------|---------------------|---------------------|----------------------|----------------------|
| 10 | 21 | 1377 | 1974 | 3076 | 4627 |
| | 26 | 1367 | 1943 | 3032 | 4551 |
| | 51 | 1344 | 1872 | 2917 | 4344 |
| | 101 | 1328 | 1830 | 2840 | 4197 |
| | ∞ | 1317 \pm 2 | 1794 \pm 3 | 2787 \pm 11 | 4102 \pm 26 |
| Font et al. [10] | | 1335 | 1846 | 2706 | 4100 |

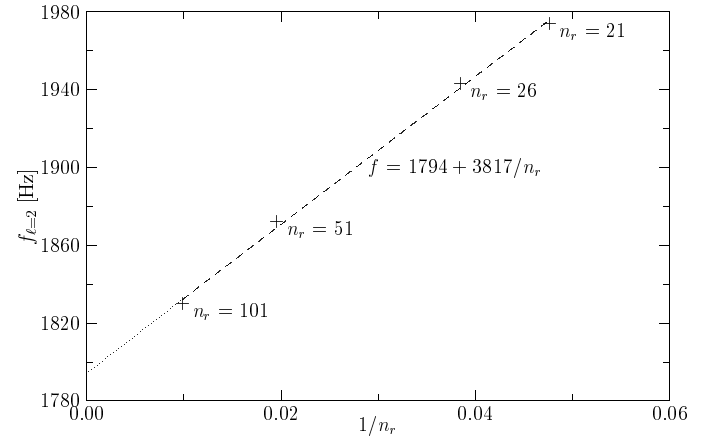


FIG. 1: The computed eigenfrequencies (here the $\ell = 2$ f -mode for BU0) follow an inverse power law. We may extrapolate to $n_r \rightarrow \infty$ to obtain the frequencies for nominally infinite radial resolution.

Comparing the extrapolated frequencies in Table II with results by Font et al. [10], we conclude that they correspond to the fundamental modes that correspond to $\ell = 0, 1, 2$ and the first pressure mode for $\ell = 2$, with an agreement up to a few percent. The remaining differences are likely be due to the finite resolution of the background calculation.

The method remains basically the same when we turn on rotation. We thus expect to obtain the fluid modes with similar accuracy even for rapid rotation. The picture may change, though, for the rotation-driven modes: These are degenerate at zero frequency in the non-rotating case. Therefore, there are no results for the non-rotating case that can be used as an indication for the accuracy of our computational results.

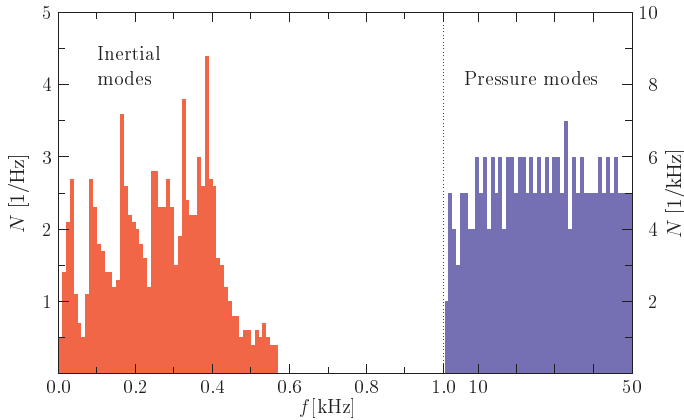


FIG. 2: A histogram of the number (per frequency bin) of all solutions returned by the eigenvalue code for the $m = 0$ eigenvalue problem of the model BU1. The frequency bins have a constant width of 10 Hz for the inertial mode frequencies and 1 kHz for the pressure mode frequencies. Note the change in frequency scale at 1kHz.

B. Rapid rotation

With rotation being included the equations of motion for the fluid become quite lengthy. Schematically they take the form

$$\begin{aligned} \Pi \frac{\partial H}{\partial t} &= \mathcal{L}_1 \left(H, f_3, f_1, f_2, \frac{\partial f_1}{\partial r}, \frac{\partial f_2}{\partial \theta}, -AC_s^2 \frac{\partial f_3}{\partial t} \right) \\ ZC_s^2 \frac{\partial f_3}{\partial t} &= \mathcal{L}_2 \left(H, f_3, f_1, f_2, \frac{\partial f_1}{\partial r}, \frac{\partial f_2}{\partial \theta}, -B \frac{\partial H}{\partial t} \right) \\ \frac{\partial f_1}{\partial t} &= \mathcal{L}_3 \left(f_3, f_1, \frac{\partial H}{\partial r} \right) \\ \frac{\partial f_2}{\partial t} &= \mathcal{L}_4 \left(f_3, f_2, \frac{\partial H}{\partial \theta} \right), \end{aligned}$$

where A,B,Z, Π are functions of the background quantities (provided in Appendix B). However, the frequency σ now appears in the matrix \mathcal{L} on the right hand side. Therefore, this form is not suitable for performing an explicit eigenvalue calculation as described in Subsection II C. We thus define new variables:

$$\begin{aligned} F &= \Pi H + AC_s^2 f_3 \\ V &= ZC_s^2 f_3 + BH, \end{aligned}$$

which together with f_1, f_2 form the set of variables we will use from now on. The full set of equations is provided in Appendix B.

In Fig. 2 we show all solutions returned by the eigenvalue code for axisymmetric perturbations of model BU1, using a low radial resolution of $n_r = 25$. As far as results for pressure modes are available from the literature we list them along with our results in Table III. No previous results are available for axisymmetric inertial modes of rapidly rotating relativistic stars; see Ruoff et

al. [25] for modes of slowly rotating stars. Very recently Dimmelmeier et al. [9] published frequencies of the three strongest axisymmetric inertial modes in the conformally flat approximation. They all lie inside the corresponding inertial mode spectrum (see below).

We notice from Fig. 2 that the eigenvalues are clustered into two groups, one above 1000Hz and one below. These correspond to the expected frequency ranges for pressure modes and inertial modes. The latter range is more densely populated; for example, we see more solutions between, say, 500 and 520 Hz than between 2 and 5 kHz. This is not as surprising as it may seem at first: according to theory (see eg. [19] for an overview table), there is an infinite number of pressure modes, with frequencies extending to infinity. For the inertial modes though, one expects an infinite number of modes as well, but confined to a well defined frequency range. According to our computation this range appears to extend from 0 to about 600 Hz for the model BU1.

In Figs. 3 and 4 we show the p -mode and inertial mode ranges separately for increasing radial resolution. In both ranges the number of frequency eigenvalues increases with increasing resolution. There is an important distinction, however: in the p -mode range, higher frequency ranges are increasingly populated as the resolution increases, while the population of low frequencies approaches a limiting value. We observe that as the radial resolution n_r increases, the number of computed eigenvalues increases as $10 \times n_r$. The lowest p -mode frequency, which belongs to the $m = 2$ f -mode, is roughly the same for all resolutions. It shifts in frequency by a few hundred Hz, which is just a few percent of the bin size. Typically the number of solutions per frequency bin approaches a limit value α like $N_{\text{bin}} \approx \alpha + \beta/n_r$ with some constant β .

For each stellar model the maximum value of frequency eigenvalues tends to infinity for increasing resolution. This is similar to the situation for quasi-normal modes of black holes, with an infinite number of modes which is not confined to a finite part of the complex frequency plane (see [22]). In the case of black holes, however, the imaginary part of the frequency is unbounded, while it is the real (oscillatory) part of the frequency for pressure

TABLE III: Frequencies (in kHz) of two fundamental $m = 0$ pressure-driven oscillations for the polytropic models BU1 and BU6, compared with the results of [10]. In the non-rotating limit these correspond to $l = 0$ and $l = 2$ modes. Again, our values have been extrapolated to nominally infinite radial resolution. Convergence in this case was not as clean as shown in Fig. 1, especially for the rapidly rotating model BU6. This is reflected in larger uncertainty estimates.

| | $f_{l=0}$ (BU1) | $f_{l=2}$ (BU1) | $f_{l=0}$ (BU6) | $f_{l=2}$ (BU6) |
|------------------|-----------------|-----------------|-----------------|-----------------|
| This paper | 2.720 ± 20 | 1.834 ± 25 | 2.292 ± 193 | 1.718 ± 85 |
| Font et al. [10] | 2.657 | 1.855 | 2.456 | 1.762 |

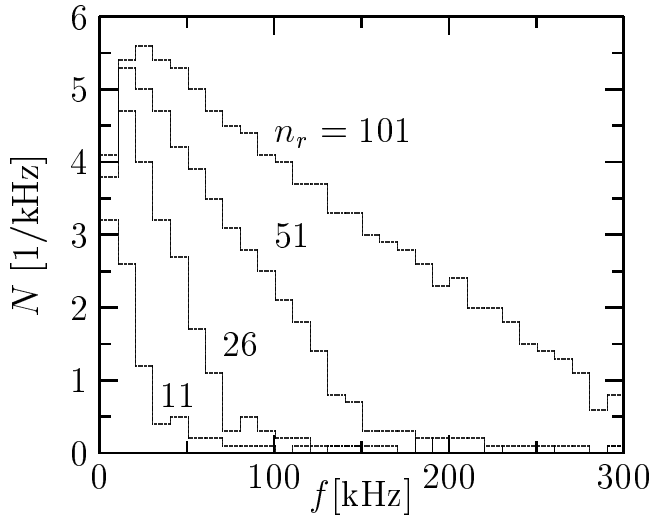


FIG. 3: A histogram of the number of p-modes per frequency bin computed for the $m = 0$ eigenvalue problem of the model BU1. The bins are equally sized at 10kHz

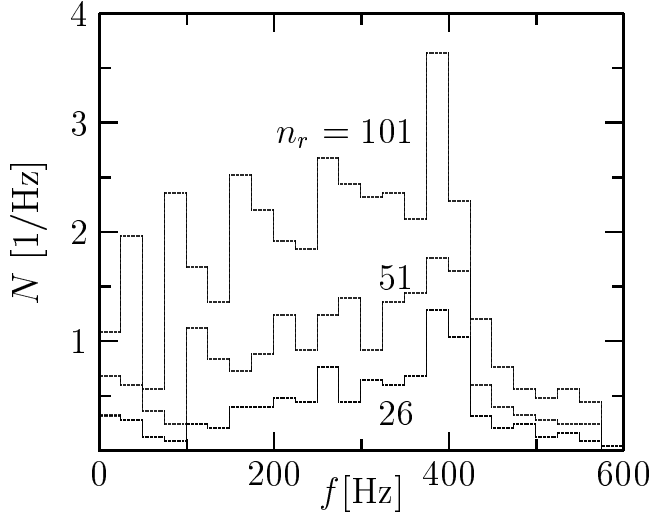


FIG. 4: The same as for figure 3 but for the inertial modes of the same problem. The bin size is now 25Hz

modes of relativistic stars.

In the inertial mode range, on the other hand, the frequency range does not change as the resolution increases; in fact, the upper limit (600Hz for model BU1) is quite robust. Instead, the population increases fairly homogeneously over the whole frequency range. The total number of solutions calculated develops, just as for the p-modes, like $10 \times n_r$. The number of points per bin grows linearly; for the bin e.g. around 400Hz, as $N_{\text{bin}} \simeq 2 \times n_r$. This is a strong indication that an infinite number of solutions exists in this frequency range. It would seem likely that there is an infinite number of physical modes in this range as well.

While the upper limit for the frequency range does not depend on the resolution used in the numerical calculation, it actually depends linearly on the rotational

frequency of the star, as shown in Fig. 5. The linear fit reveals $\sigma_{\text{max}} = 0.257 \times \Omega$ with a negligible statistical error.

The picture in Fig. 3 is actually quite common for numerical studies of oscillation spectra: as one increases the resolution, frequency ranges at increasingly higher frequency become populated, while there is a finite limit for lower frequency ranges. Usually one expects that at low resolution, only modes with low frequencies can be computed reliably, since they are the only ones which can be resolved sufficiently well. Numerical solutions at high frequencies are likely spurious and cannot be trusted. With increasing resolution, the number of reliable solutions increases and their range extends to higher frequencies.

On the other hand, if we are confronted with a finite frequency range which shows an increasing number of solutions with increasing resolution, such a distinction cannot be made in a meaningful way. It is therefore not clear which of the numerical solutions in the frequency range corresponding to inertial modes should be considered physical solutions, and which should be discarded as numerical artefacts.

Just as in the non-rotating case, one can establish convergence for any finite value of the frequency in the upper range (Fig. 3), since there is a finite number of distinct modes in any finite frequency interval. The limit values very likely correspond to physical modes of the star. In the lower frequency range (Fig. 4) it is not even clear how to establish a correspondence between eigenvalues at increasing resolutions, let alone define convergence and establish a correspondence to physical modes. However, given our numerical results, we consider it likely that the frequency range from 0 to 600 Hz does *not* contain only a *finite* number of inertial modes, in agreement with theoretical expectations. This leaves the following possibilities: There may be an infinite number of discrete frequencies, there may be a continuous spectrum, or a combination of these two. Note that an infinite number of frequencies in a finite frequency range implies the existence of at least one accumulation point. Such an accumulation point must be part of a continuous spectrum. A common example is the spectrum of a highly excited atom: it has an accumulation point at zero energy, which marks the edge of the continuous spectrum. However, the numerical limitations do not allow us to draw more specific conclusions, such as to the extent of a continuous spectrum, whether there are discrete modes in addition, where they may be, etc. The rather uneven distribution of solutions across the frequency range in question is an indication, though, that the actual spectrum may be far from having a simple structure.

IV. NON-AXISYMMETRIC PERTURBATIONS

For $m > 0$ the picture is more complicated but also more interesting than the axisymmetric case since the $m = 2$ modes are the ones most unstable to gravitational

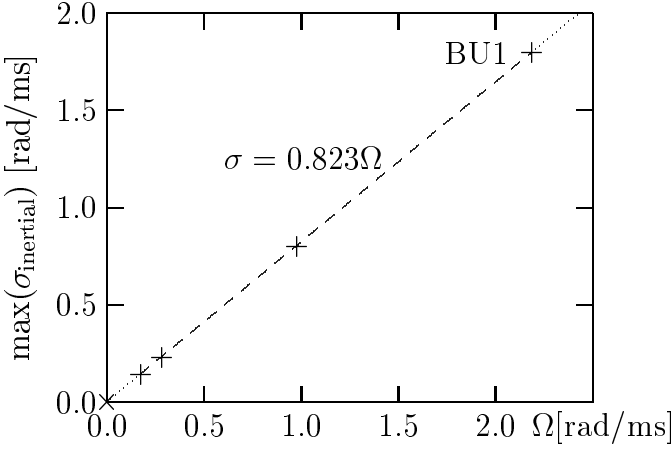


FIG. 5: The highest inertial mode frequency as a function of the star's rotational frequency, starting at the model BU0 (no rotation) and moving up to model BU1 (2185Hz).

radiation. Solving this system for $m = 2$ and the BU1 model in the way described in the previous section we find a set of eigenvalues, containing both positive and negative frequencies. In the axisymmetric case negative eigenvalues are equivalent to the positive frequency solutions. Breaking axial symmetry shifts frequencies (for an asymptotic observer) towards negative values, so that much or even all of the frequency range corresponding to inertial modes becomes negative.

In Newtonian gravity (see e.g. Unno et al. [28]), a polar mode of order n , harmonic index ℓ and frequency σ_0 , splits under rotation to $2\ell + 1$ modes with frequencies shifted to $\sigma = \sigma_0 - m\Omega E_{n\ell}$ ($+O(\Omega^2)$) where $E_{n\ell}$ is a function depending on the eigenfunction of each mode. For low order pressure modes the value of this function is about 0.1, so one would need rotational frequencies close to the Kepler limit for the frequency to change sign.

However, there are modes which have $\sigma < 0$ for *any* rotation rate, such as the *r*-modes which in the Newtonian, slow-rotation limit have $\sigma = -2m\Omega \frac{(\ell-1)(\ell+2)}{\ell(\ell+1)}$. This is the picture we find for $m = 2$, with all inertial modes having negative frequencies. Such a change of sign is often used as an indication for the corresponding mode to become unstable [see eg. 27].

In Fig. 5 we saw that the upper cutoff frequency for the inertial mode range grows linearly with the rotational frequency of the star. In the non-axisymmetric case, there is also a dependence on m . For the series of models listed in Table I we obtain a least square fit of $\sigma_{\max} = \Omega(1.6 - 1.05m)$, with statistical errors of about 0.1 for both values. For less relativistic models with a central energy density 1/10 that of BU1, this changes to $\sigma_{\max} = \Omega(1.93 - 1.03m)$, close to what Lindblom and Ipser [17] predicted and Brink et al. [7] found for Newtonian stars where $\sigma_{\max} \approx \Omega(2 - m)$.

In the axisymmetric case a zero-frequency mode in the

rotating frame has 0 Hz also for an inertial observer, it corresponds to the mid-point of the inertial mode frequency range. For non-axisymmetric perturbations the center of the spectrum is expected to shift to $-m\Omega$, which indeed appears to be the case in our results. The corresponding inertial mode spectrum for a specific azimuthal index $m > 0$ is however not completely symmetric since modes with different order n or harmonic indices ℓ have different frequency shifts. This shift is rather small for pressure modes. As the azimuthal index m can take arbitrarily large values, the inertial modes can, according to the above, reach arbitrarily large negative frequencies. Since these are equivalent to positive frequencies with a phase difference, the frequency range of inertial modes will overlap with that of pressure modes. An overview of the spectra for three different values of the azimuthal index m can be seen in Fig. 6.

The oscillation frequencies are influenced not only by changes in the equilibrium configuration of the star, but by other effects as well, such as the frame dragging at the surface and the center [15]. These also scale linearly with Ω . Knowing the range of inertial mode frequencies as a function of the star's rotational period in advance may be quite helpful for actual observations of gravitational radiation emitted by these oscillations. The frequencies of individual modes, such as the fundamental *r*-mode, are not examined here and form the focus of a forthcoming paper.

V. CONCLUSIONS

We have presented the first numerical calculation of oscillation frequencies of rapidly rotating relativistic stars for both axisymmetric and non-axisymmetric perturbations, using the relativistic Cowling approximation.

For the polytropic equations of state that we have employed here, we found an infinite set of pressure modes with a range of frequencies bounded only from below at about 2kHz. In addition, there is a presumably infinite set of solutions at lower frequencies in a well defined range which corresponds to inertial modes. In the axisymmetric case ($m = 0$) this frequency range is symmetric around zero. It extends to a maximum frequency which depends linearly on the star's rotation rate ν_{star} and approaches $2\nu_{\text{star}}$ for less relativistic stars. For non-axisymmetric perturbations oscillation frequencies shift towards negative numbers. This affects pressure modes only slightly, while the inertial modes now all have frequencies below zero.

It is not clear whether this low-frequency part of the spectrum is discrete or continuous, or a combination of both. The dense and somewhat uneven distribution of the eigenvalues is an indication that the actual structure of the physical spectrum may be quite complicated. Further investigation is needed into the question how a spectrum with a continuous part can be studied numerically. Furthermore, explicit time evolution of perturbations of

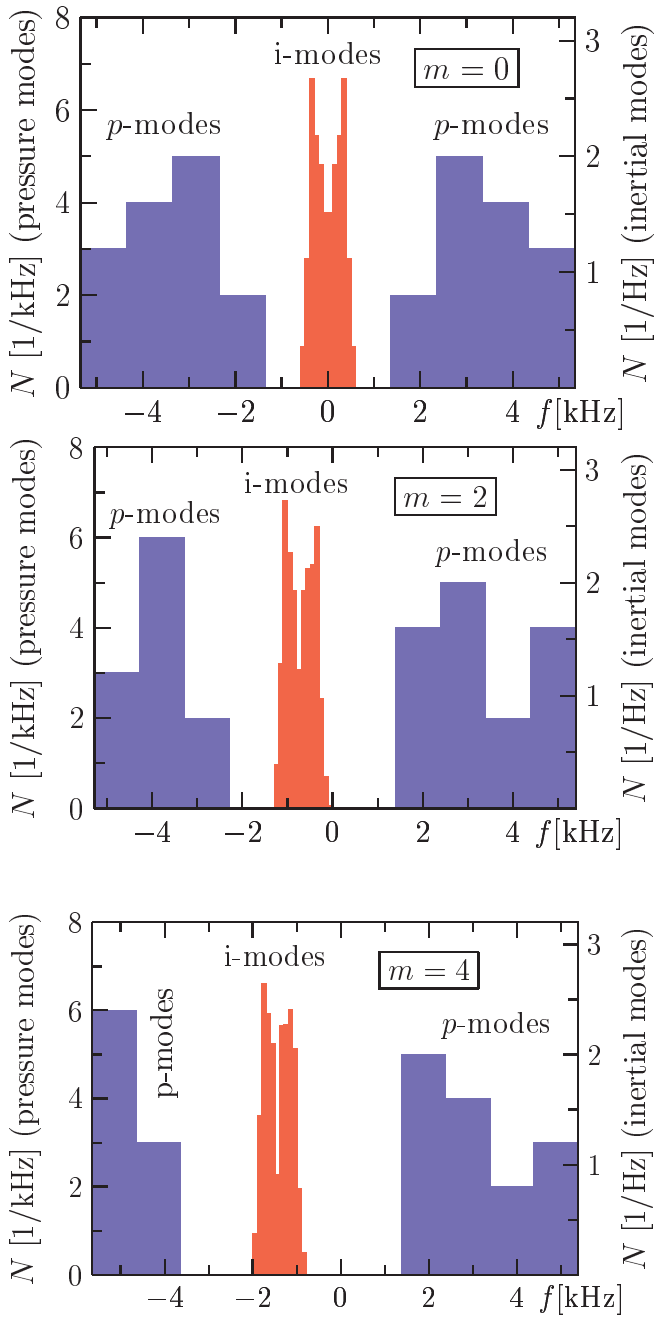


FIG. 6: The histogram of both positive and negative solutions of the eigenvalue code for $m = 0, 2$, and 4 . The values for the inertial modes (middle) are scaled differently for better presentation.

the same configurations could provide an independent means of studying their spectrum and checking the results we have presented here. Identification of individual modes in this part of the spectrum will be studied in a forthcoming paper.

Applying realistic equations of state requires only slight modification of the code and will shift the frequencies to some extent, but the overall picture should remain the same. The effect of a non-barotropic equation of state on the inertial mode spectrum presents a very interesting question for further study.

Finally, for an accurate calculation of the oscillations frequencies, the disposal of the Cowling approximation will be necessary. This is important not just to avoid deviation of the calculated frequencies introduced by the Cowling approximation, which we expect to be small, but also to ensure the consistency of the problem (see Section I). The major problem lies not in the perturbation equations becoming more complex, but in defining the boundary conditions in the spacetime outside the star. Observation of potentially unstable modes with the now-operational gravitational-wave detectors is possible only if precise knowledge of these modes is available as a basis for the analysis of the gravitational wave data.

Acknowledgments

This work was supported by the german science foundation (DFG), via a SFB/Transregio. We are grateful to Prof. K. Kokkotas for significantly contributing to accomplishing this work. P.D. Dr. J. Frauendiener from the University of Tübingen and Prof. N. Stergioulas from the University of Thessaloniki gave key advice concerning numerical procedures.

- [1] N. Andersson, *Astroph. J.* **502**, 708 (1998), gr-qc/9706075
- [2] N. Andersson, *Class. Quant. Grav.* **20**, 105 (2003), astro-ph/0211057
- [3] N. Andersson and K. Kokkotas, *Mon. Not. R. Astron. Soc.* **308**, 745 (1999), gr-qc/9903019

- Soc. **299**, 1059 (1998), gr-qc/9711088
- [4] N. Andersson and K. Kokkotas, *Int. J. Mod. Phys. D* **10**, 381–442 (2001), gr-qc/0010102
- [5] H. R. Beyer and K. D. Kokkotas, *Mon. Not. R. Astron. Soc.* **308**, 745 (1999), gr-qc/9903019

[6] S. Boutloukos, J. Ph. C. S. **8**, 81 (2005)

[7] J. Brink, S. A. Teukolsky and I. Wasserman, Phys. Rev. D **70**, 124017 (2004), gr-qc/0409048

[8] T. G. Cowling, Mon. Not. R. Astron. Soc. **101**, 367 (1941)

[9] H. Dimmelmeier, N. Stergioulas, and J. A. Font, astro-ph/0511394

[10] J. A. Font, H. Dimmelmeier, A. Gupta and N. Stergioulas, Mon. Not. R. Astron. Soc. **325**, 1463 (2001), astro-ph/0012477

[11] R. Emden "Gaskugeln", Teubner, Leipzig (1907)

[12] L. S. Finn, Mon. Not. R. Astron. Soc. **232**, 259 (1988)

[13] J. L. Friedman and B. F. Schutz, Astroph. J. **221**, 937 (1978)

[14] K. Kokkotas and B. Schmidt, Liv. Rev. Rel. **2**, 2 (1999), gr-qc/9909058

[15] Y. Kojima and M. Hosonuma, Astroph. J. **520**, 788 (1999), astro-ph/9903055

[16] D. Lai, Mon. Not. R. Astron. Soc. **307**, 1001 (1999), astro-ph/9806378

[17] L. Lindblom and J. R. Ipser, Phys. Rev. D **59**, 044009 (1999), gr-qc/9807049

[18] K. H. Lockitch, N. Andersson and J. L. Friedman, Phys. Rev. D **63**, 024019 (2001), gr-qc/0008019

[19] K. H. Lockitch, N. Andersson and A. Watts, Class. Quant. Grav. **21**, 4661–4676 (2004), gr-qc/0106088

[20] K. H. Lockitch and J. L. Friedman, Astroph. J. **521**, 764 (1999), gr-qc/9812019

[21] K. H. Lockitch, J. L. Friedman and N. Andersson, Phys. Rev. D **68**, 124010 (2003), gr-qc/0210102

[22] H.-P. Nollert, Phys. Rev. D **47**, 5253 (1993)

[23] H.-P. Nollert, Class. Quant. Grav. **16**, 159 (1999)

[24] J. Provost, G. Berthomieu and A. Rocca, Astron. Astroph. **94**, 126–133 (1981)

[25] J. Ruoff, A. Stavridis and K. Kokkotas, Mon. Not. R. Astron. Soc. **339**, 1170 (2003), gr-qc/0203052

[26] N. Stergioulas and J. L. Friedman, Astroph. J. **444**, 306 (1995), astro-ph/9411032

[27] N. Stergioulas, Liv. Rev. **6**, 3 (2003), gr-qc/0302034

[28] W. Unno, Y. Osaki, H. Ando and H. Shibahashi, *Non-radial Oscillations of Stars*, Tokyo: University Press (1989)

[29] S. Yoshida and Y. Kojima, Mon. Not. R. Astron. Soc. **289**, 117 (1997), gr-qc/9705081

[30] S.-I. Yoshida and Y. Eriguchi, Astroph. J. **515**, 414 (1999), astro-ph/9807254

[31] S.-I. Yoshida, S. Yoshida and Y. Eriguchi, Mon. Not. R. Astron. Soc. **356**, 217 (2005), astro-ph/0406283

[32] For isentropic stars this holds for all the modes only in the non-rotating limit.

[33] The $e^{im\phi}$ -dependency of non-axisymmetric fluid perturbations requires that on the axis all possible azimuthal angles give the same value, i.e. zero.

APPENDIX A: DISCUSSION OF SOME NUMERICAL DIFFICULTIES

The Cowling approximation does not include the damping of oscillations by emission of gravitational waves, and no other damping mechanism is included in our models. Therefore, all eigenfrequencies should be purely real. However, the code we use is designed for calculating complex frequencies. The imaginary parts of the computed values should therefore turn out to be close to zero, on the order of machine accuracy ($\sim \leq 10^{-14}$). This is indeed the case for the majority of the solutions we found. Some of the eigenvalues in the frequency range of modes, however, have a non-negligible imaginary part of $\sim \leq 1\%$ of the real part.

We are thus facing the question if some error occurred in the implementation of the perturbation equations into the code. The perturbation equations were first computed using Maple. The resulting expressions were then simplified by hand and implemented numerically. As an alternative, we inserted the Maple output directly into the code without any simplification. The spurious imaginary parts of inertial mode frequencies then became larger, rather than smaller. We are therefore confident that they are not the result of some actual error in implementing the equation, but a consequence of truncation error, especially in conjunction with a bad numerical condition of the coefficient matrix \mathcal{A} .

Deviations from the expected convergence were found, while eigenfunctions were also seen to be changing form in the rotating case. Testing our code by relabeling the eigenvectors revealed the same results, which strengthens its correctness. Still, considerably more work is required to clarify the question how numerical results can help to reveal the complicated structure of the spectrum we are studying here.

APPENDIX B: THE FULL SYSTEM OF EQUATIONS FOR THE FLUID PERTURBATIONS

$$\begin{aligned}
\partial_t F = & \frac{imF}{Z\Pi - AB} \left\{ B \frac{[e^{2\rho} + r^2 \sin^2 \theta \omega(\Omega - \omega)]^2 + e^{2\rho} \Omega^2 r^2 \sin^2 \theta}{r^2 \sin^2 \theta e^{\gamma+\rho} u^0} - (1 + C_s^2) \Omega Z [e^{2\rho} + r^2 \sin^2 \theta \omega(\Omega - \omega)] \right\} \\
& - \frac{imV}{Z\Pi - AB} \left\{ \Pi \frac{[e^{2\rho} + r^2 \sin^2 \theta \omega(\Omega - \omega)]^2 + e^{2\rho} \Omega^2 r^2 \sin^2 \theta}{r^2 \sin^2 \theta e^{\gamma+\rho} u^0} - (1 + C_s^2) \Omega A [e^{2\rho} + r^2 \sin^2 \theta \omega(\Omega - \omega)] \right\} \\
& - C_s^2 u^0 \frac{e^{\gamma-\rho}}{e^{2\alpha}} \left\{ \frac{e^{2\rho} + r^2 \sin^2 \theta \omega(\Omega - \omega)}{(u^0)^2 e^{\gamma-\rho}} \left(\frac{3}{2} \partial_r \gamma - \frac{1}{2} \partial_r \rho + \frac{3}{r} \right) - r^4 \sin^4 \theta (\Omega - \omega)^3 \partial_r \omega \right. \\
& \left. - e^{2\rho} r^2 \sin^2 \theta \left[\omega \partial_r \omega + \Omega(\Omega - \omega) \left(\partial_r \rho - \frac{1}{r} \right) \right] + \frac{e^{2\rho}}{(u^0)^2 e^{\gamma-\rho}} \left(\partial_r \rho - \frac{1}{r} \right) \right\} f_1 \\
& - \frac{C_s^2}{r^2} u^0 \frac{e^{\gamma-\rho}}{e^{2\alpha}} \left\{ \frac{e^{2\rho} + r^2 \sin^2 \theta \omega(\Omega - \omega)}{(u^0)^2 e^{\gamma-\rho}} \left(\frac{3}{2} \partial_\theta \gamma - \frac{1}{2} \partial_\theta \rho + 2 \cot \theta \right) - r^4 \sin^4 \theta (\Omega - \omega)^3 \partial_\theta \omega + \right. \\
& \left. - e^{2\rho} r^2 \sin^2 \theta [\Omega(\Omega - \omega) (\cot \theta - \partial_\theta \rho) - \omega \partial_\theta \omega] + \frac{e^{2\rho}}{(u^0)^2 e^{\gamma-\rho}} (\partial_\theta \rho - \cot \theta) \right\} f_2 \\
& - \frac{C_s^2}{u^0} e^{-2\alpha} [e^{2\rho} + r^2 \sin^2 \theta \omega(\Omega - \omega)] \left(\partial_r f_1 + \frac{1}{r^2} \partial_\theta f_2 \right) \tag{B1}
\end{aligned}$$

$$\begin{aligned}
\frac{\partial V}{\partial t} = & - \frac{im}{Z\Pi - AB} \left\{ B \left(\frac{\omega}{(u^0)^2 e^{\gamma-\rho}} - 2\Omega e^{2\rho} \right) + u^0 e^{\gamma+\rho} Z [C_s^2 e^{2\rho} + r^2 \sin^2 \theta (\Omega - \omega) (C_s^2 \omega + \Omega)] \right\} F \\
& + \frac{im}{Z\Pi - AB} \left\{ \Pi \left(\frac{\omega}{(u^0)^2 e^{\gamma-\rho}} - 2\Omega e^{2\rho} \right) + u^0 e^{\gamma+\rho} A [C_s^2 e^{2\rho} + r^2 \sin^2 \theta (\Omega - \omega) (C_s^2 \omega + \Omega)] \right\} V \\
& - C_s^2 r^2 \sin^2 \theta \frac{\Omega - \omega}{e^{2\alpha}} e^{\gamma+\rho} \left\{ \frac{3}{2} \partial_r \gamma - \frac{1}{2} \partial_r \rho + \frac{3}{r} + (u^0)^2 e^{\gamma+\rho} \left[-\partial_r \rho + \partial_r \ln (\Omega - \omega) + \frac{1}{r} \right] \right\} f_1 \\
& - C_s^2 \sin^2 \theta \frac{\Omega - \omega}{e^{2\alpha}} e^{\gamma+\rho} \left\{ \frac{3}{2} \partial_\theta \gamma - \frac{1}{2} \partial_\theta \rho + 2 \cot \theta + (u^0)^2 e^{\gamma+\rho} [-\partial_\theta \rho + \partial_\theta \ln (\Omega - \omega) + \cot \theta] \right\} f_2 \\
& - C_s^2 r^2 \sin^2 \theta (\Omega - \omega) e^{\gamma+\rho} e^{-2\alpha} \left(\partial_r f_1 + \frac{1}{r^2} \partial_\theta f_2 \right) \tag{B2}
\end{aligned}$$

$$\begin{aligned}
\partial_t f_1 = & \left\{ \frac{B}{C_s^2} \frac{2(\Omega - \omega) (\partial_r \rho - \frac{1}{r}) + e^{-2\rho} Z \partial_r \omega}{Z\Pi - AB} + \frac{\partial_r \ln (p + \epsilon)}{u^0 (\Pi - AB/Z)} - \frac{1}{u^0} \partial_r \left(\frac{Z}{Z\Pi - AB} \right) \right\} F \\
& - \left\{ \frac{\Pi}{C_s^2} \frac{2(\Omega - \omega) (\partial_r \rho - \frac{1}{r}) + e^{-2\rho} Z \partial_r \omega}{Z\Pi - AB} + \frac{\partial_r \ln (p + \epsilon)}{u^0 (Z\Pi/A - B)} - \frac{1}{u^0} \partial_r \left(\frac{A}{Z\Pi - AB} \right) \right\} V \\
& - \frac{\partial_r F}{u^0 (\Pi - AB/Z)} + \frac{\partial_r V}{u^0 (Z\Pi/A - B)} - im\Omega f_1 \tag{B3}
\end{aligned}$$

$$\begin{aligned}
\partial_t f_2 = & \left\{ \frac{B}{C_s^2} \frac{2(\Omega - \omega) (\partial_\theta \rho - \cot \theta) + e^{-2\rho} Z \partial_\theta \omega}{Z\Pi - AB} + \frac{\partial_\theta \ln (p + \epsilon)}{u^0 (\Pi - AB/Z)} - \frac{1}{u^0} \partial_\theta \left(\frac{Z}{Z\Pi - AB} \right) \right\} F \\
& - \left\{ \frac{\Pi}{C_s^2} \frac{2(\Omega - \omega) (\partial_\theta \rho - \cot \theta) + e^{-2\rho} Z \partial_\theta \omega}{Z\Pi - AB} + \frac{\partial_\theta \ln (p + \epsilon)}{u^0 (Z\Pi/A - B)} - \frac{1}{u^0} \partial_\theta \left(\frac{A}{Z\Pi - B} \right) \right\} V \\
& - \frac{\partial_\theta F}{u^0 (\Pi - AB/Z)} + \frac{\partial_\theta V}{u^0 (Z\Pi/A - B)} - im\Omega f_2 \tag{B4}
\end{aligned}$$

where

$$\begin{aligned}
A &= \left(2\Omega e^{2\rho} - \frac{\omega}{(u^0)^2 e^{\gamma-\rho}} \right) \frac{1}{e^{\gamma+\rho} u^0} \\
B &= r^2 \sin^2 \theta (\Omega - \omega) e^{\gamma+\rho} u^0 (1 + C_s^2) \\
\Pi &= e^{2\rho} + r^2 \sin^2 \theta (\Omega - \omega) (C_s^2 \Omega + \omega) \\
Z &= e^{2\rho} + r^2 \sin^2 \theta (\Omega - \omega)^2
\end{aligned}$$

and $\partial_r, \partial_\theta$ stand for the partial derivatives with respect to r and θ .